ARCHIVES
of
FOUNDRY ENGINEERING

ISSN (2299-2944)
Volume 2025
Issue 4/2025

167 – 174

22/4

10.24425/afe.2025.157615

Published quarterly as the organ of the Foundry Commission of the Polish Academy of Sciences

# The Influence of Microstructure on the Corrosion Properties of Selected Magnesium Alloys

**W. Wyrwa *, K. Naplocha**
Wrocław University of Science and Technology, Poland
* Corresponding author: E-mail address: wojciech.wyrwa@pwr.edu.pl

Received 02.07.2025; accepted in revised form 29.08.2025, available online 31.12.2025

## Abstract

This work aimed to evaluate the corrosion resistance of selected magnesium alloys in 3.5 % NaCl solution at room temperature and to determine the influence of microstructure on this property. For this purpose, SEM microscope with the EDS/EDX system and electrochemical measurements (LSV, EIS) have been employed. The following materials have been selected – binary Mg-Zn alloy with 3% content of zinc, AZ91 manufactured by gravity and squeeze casting. It has been concluded that corrosion resistance follows the order AZ91(SQ) > AZ91 (AC) > MgZn3. Based on obtained measurements data the equivalent electrical circuit for tested materials has been presented and values of its parameters have been determined using computer fitting and simulation. Furthermore, it has been stated that after squeeze casting, the microstructure of AZ91 is more refined and $Mg_{17}Al_{12}$ phase is in a form of continuous network compared to samples produced by gravity casting. For these reasons, in this comparison the best corrosion resistance is demonstrated by AZ91 after squeeze casting because $Mg_{17}Al_{12}$ phase acts as an inhibitor and decreases the corrosion rate in this case. MgZn3 demonstrates the lower corrosion resistance due to the lack of Al in the chemical composition.

**Keywords:** Magnesium alloys, Squeeze casting, Corrosion properties, Electrochemical impedance spectroscopy

## 1. Introduction

Magnesium based alloys, due to their low density, lightweight nature, high specific strength, low cost and presenting in abundance on the earth, appear very attractive for many industry and engineering fields. For instance, employed automobiles and aerospace applications, or developed seawater battery. Moreover, in biomedical engineering as an orthopedic biodegradable implants because of their biocompatibility and mechanical properties similar to natural bone. However, the application of magnesium alloys is restricted due to insufficient corrosion resistance with exceedingly low standard electrode potential of Mg (-2.37 V) and hydrogen evolution during corrosion processes. Furthermore, they are susceptible to dissolution in aqueous solutions, especially in those containing chloride ions [1–8].

Some of the most important alloying elements commonly used for magnesium are aluminum and zinc. The chemical composition of the alloy and the method of its manufacture influence its microstructure, which plays a key role in determining its corrosion resistance [1].

In general, obtained alloys consist of α-Mg matrix. Apart from that there is a second β-phase, which may have a dual role in the corrosion behavior of the material – a galvanic acceleration effect or a corrosion blocking effect, depending on its properties, distribution and amount. The β-phase has a nobler potential compared to the magnesium matrix and can act as a cathode in relation to α-Mg, what implies galvanic corrosion. However,

when it is in a finer and continuous form, β-phase can act as an inhibitor and decrease the corrosion rate [4, 9–13].

Aluminum improves the corrosion resistance of magnesium alloys through forming a protective layer on the surface, and it also reduces hydrogen evolution compared to pure magnesium. Furthermore, it forms β-$Mg_{17}Al_{12}$ phase, which is crucial for the properties of the alloy. Whereas, zinc helps to refine the grain size, improving its mechanical properties and contributing to better corrosion resistance. Mg-Al-Zn alloys are commonly known as AZ series alloys [1]. For instance, in the automotive sector, the AZ91 alloy is the most commonly employed casting alloy, making up almost 90% of all magnesium casting products [2, 14–16].

Such alloy consists of the α-Mg matrix and intermetallic β-$Mg_{17}Al_{12}$ phase distributed at the grain boundary. The volume fraction and morphology of the $Mg_{17}Al_{12}$ phase play a crucial role in the mechanical strengthening, castability, and corrosion protection of these alloys [2, 17–20].

In many studies [2, 9, 21–25] it has been investigated and confirmed that the greater content of $Mg_{17}Al_{12}$ implies a decrease in corrosion rate. This phase might improve corrosion resistance by acting as a barrier surface that prevents dissolution of the anodic α-Mg matrix area. It also establishes a protective layer that inhibits corrosion by strengthening the surface oxide film and minimizing galvanic interactions. However, a further increase in the aluminum (and also β phase) content can also develop local galvanic cells, thereby leading to the emergence of brittle phases that might reduce corrosion resistance over time [1, 26]. Thus, $Mg_{17}Al_{12}$ phase influences corrosion resistance but decrease in corrosion rate depends on its microstructure and amount.

Madhavan et al. [1] compared corrosion properties of AZ31, AZ61 and AZ91 magnesium alloys that differed from each other in the content of Al. Based on their investigation (including electrochemical impedance spectroscopy) in 3.5 % NaCl solution, it has been stated that AZ61, which contained moderate amount of Al, had the highest corrosion resistance and the lowest corrosion rate. The values of the parameters, calculated for proposed equivalent electrical circuit and obtained thanks to potentiodynamic polarization, indicated that this property changed in the order AZ61 > AZ91 > AZ31. Unfortunately, in this work there is no information about the casting technology used to manufacture analyzed alloys.

Marodkar et al. [2] investigated AZ91 samples obtained through gravity die casting, squeeze casting and extrusion. In this work it has been concluded that after squeeze casting the AZ91 alloy had a lower corrosion rate in 3.5 % NaCl solution than after gravity casting and it has been stated that β-$Mg_{17}Al_{12}$ phase increases corrosion resistance but when is in a finer form. In case of a bulky and isolated microstructure, this phase can accelerate degradation due to galvanic couple effect. It should be underlined that the squeeze casting process refines the microstructure what has been shown in these investigations. Additionally, in this work, the best corrosion resistance determined for the extrusion sample due to the absence of porosity, refinement and some amount of dissolved β-$Mg_{17}Al_{12}$ in the matrix region. Hence it can be concluded that to improve corrosion resistance, alteration of the β-$Mg_{17}Al_{12}$ phase morphology is necessary.

A distinct group of materials are binary Mg–Zn alloys, in which there is β-MgZn phase in the microstructure. Zinc can improve the corrosion resistance and mechanical properties of magnesium alloys [3]. According to the Mg–Zn binary phase diagram [27], the maximum solid solubility of Zn in Mg is 6.2 % at the eutectic temperature 341 °C. Hence, various contents of Zn, to even 7%, and their influence alloy parameters have been investigated in many studies. It should be added here that with an increase in the amount of zinc in the describing range, the percentage of β-MgZn phase is higher.

Boehlert et al. [28] conducted investigations on alloys with Zn amount ranging from 0 to 4.4 wt.% and stated that the optimal content of this element which improves mechanical parameters (tensile and creep properties) is 4% and the improvement mechanism corresponding to fine grain strengthening, solid solution strengthening and second phase strengthening.

Shuhua et al. [4] performed electrochemical measurements and concluded that corrosion resistance increases with a higher Zn content in the range of 1 - 5%. Further increase of this element to 7% results in higher corrosion rate values due to the galvanic couple effect. For alloys with 5% and 7% content of zinc, MgZn intermetallic phase was in the form of a continuous network structure. However, a greater amount of this element implies a higher volume percent of this phase, which can accelerate hydrogen evolution rate.

This paper aimed to investigate the microstructure of selected magnesium alloy castings and to compare their corrosion properties using electrochemical measurements. The relationship between these parameters has been also evaluated. As corrosion environment employed 3.5 % NaCl solution at room temperature. The selected and used in the research materials have been presented in Table 1 below where there are information about proposed abbreviations for them and about their manufacturing process. Furthermore, the basic differences between them have been presented in Table 1.

Table 1.
The proposed abbreviations for investigated materials employed in this work and their basic properties.

| Abbreviation | Alloy | Fabrication process | Al content | Zn content |
|---|---|---|---|---|
| AZ91 (AC) | AZ91 | gravity casting | 9 wt. % | 1 wt. % |
| AZ91 (SQ) | AZ91 | squeeze casting | 9 wt. % | 1 wt. % |
| MgZn3 | binary Mg-Zn alloy | gravity casting | 0 wt. % | 3 wt. % |

# 2. Materials and Methods

## 2.1. Materials

For samples preparation employed commercially available as-cast AZ91 alloy manufactured by gravity casting, which chemical composition presented in Table 2. Based on this AZ91 (AC) samples have been fabricated. To prepare squeeze cast alloy AZ91 (SQ) above material has been remelted to temperature 720

°C in a steel crucible under a protective SF6 atmosphere to avoid oxidation. A steel preform had been preheated at 300 °C. The melt was squeezed for 15 s at 150 MPa pressure. Whereas MgZn3 samples manufactured with high-purity raw material. At first, magnesium was melted in a resistance furnace. Next, preheated zinc at temperature 80 °C has been added and the melt was heated at 720 °C again. Process conducted under a protective SF6 atmosphere and by continuous mechanical stirring. This alloy has been cast using investment casting method to gypsum molds. In the first step a samples shape prepared from PLA (polylactic acid) using 3D printing. Then, the gating system has been attached and this system has been inserted in the gypsum mold, which has been hardened and dried. In the next step the mold has been subjected to heat treatment in order to burn and remove organic material and to obtain a copy of the designed shape. This process conducted at three temperature levels – 180°C, 370°C, and 720°C – each held for 2 hours. The heating between these temperature steps remained 2 hours. After this preparation, the right gravity casting process has been started [29,30].

Table 2.
Chemical composition of AZ91 magnesium alloy

| Element | Mg | Al | Zn | Mn | Si |
|---|---|---|---|---|---|
| wt. % | balance | 9.00 | 1.00 | 0.13 | 0.05 |

## 2.2 Methods

The microstructure characterized by SEM images analysis, where employed Hitachi TM3000 scanning electron microscope with the EDS/EDX system (Hitachi High-Technologies Corporation, Tokyo, Japan) and Multiscan program to shadow analysis and to estimate the percentage of phases. Based on obtained SEM images providing microstructure after casting process and properties of this program the grain size of α-Mg matrix has been estimated for investigated samples. For each material at first determined ten values and then calculated the arithmetic mean with standard deviation which has been provided as a final result.

Furthermore, the hardness of tested samples has been investigated. This parameter measured five times for each material on the same sample and results provided in form of obtained arithmetic mean with standard deviation. In this stage, Brinell hardness tester employed (VEB Werkzeug-maschinenkombinat "Fritz Heckert", Leipzig, Germany) with a steel ball of 2.5 mm diameter and load of 31.25 kg.

To ascertain corrosion resistance in 3.5 % NaCl aqueous solution at room temperature employed potentiodynamic polarization (LSV – linear sweep voltammetry) and electrochemical impedance spectroscopy (EIS) using potentiostat (Metrohm Autolab BV, Ultrecht, Netherlands) working in a three-electrode system with Ag/AgCl (3M KCl) as a reference electrode. The EIS measurements conducted at OCP using a signal amplitude of 10 mV, covering a frequency range from 100 kHz down to 50 mHz. To propose electrical equivalent circuit and to determine its parameters employed Nova program.

Magnesium alloys samples polished using different grades of emery papers up to 4000 grit. Afterwards, the samples cleaned in distilled water and dried in air. Additionally, before SEM investigation the samples have been felted. Before EIS investigation tested materials immersed in ethanol for 5 minutes in a ultrasonic cleaner.

# 3. Results

## 3.1 Microstructural analysis

Figure 1 provides the surface of the investigated samples at the same magnification. The observed alloy phases marked on the SEM images using Greek letters. Magnesium matrix present in each analyzed case is represented by α. The letter β denotes for AZ91 alloys a $Mg_{17}Al_{12}$ phase but in case of MgZn3 (Figure 1c) it denotes Mg-Zn phase. The percentage fraction of the phases in the surface structure estimated using image shadow analysis which results summarized in Table 3.

Comparing SEM images for AZ91 (AC) and AZ91 (SQ) it should be stated that intermetallic $Mg_{17}Al_{12}$ phase is different. For alloy obtained by gravity casting it is bulky, separated and saturated. After squeeze casting process it creates a continuous and refined network distributed along grain boundary. The similar effect has been documented in various investigations on Mg-Al cast alloys, as noted in references [2, 31–34]. The faster solidification of molten metal due to applied pressure in the squeeze casting is responsible for the refinement of the $Mg_{17}Al_{12}$ [2, 32]. The refinement has been also observed for α-Mg matrix and γ phase containing manganese.

Table 3.
Estimated fraction of the phases in the surface structure (percent of total area)

| | **α – Mg** | **β – $Mg_{17}Al_{12}$** | **γ – MgMn** |
|---|---|---|---|
| AZ 91 (AC) | 95.0 % | 4.8 % | 0.2% |
| AZ91 (SQ) | 90.5 % | 9.4 % | 0.04 % |
| | **α – Mg** | **β – MgZn** | – |
| MgZn3 | 97.4 % | 2.6 % | – |

Based on obtained SEM images the grain size of α-Mg matrix has been estimated as 150±10 μm, 120±10 μm for AZ91 (AC) and AZ91 (SQ), respectively. This calculation additionally confirms above conclusion that squeeze casting process refined microstructure of the alloy. Finer grains of the α-Mg matrix improve both mechanical strength and corrosion resistance by increasing the density of grain boundaries, which serve as barriers to crack propagation and corrosion [1].

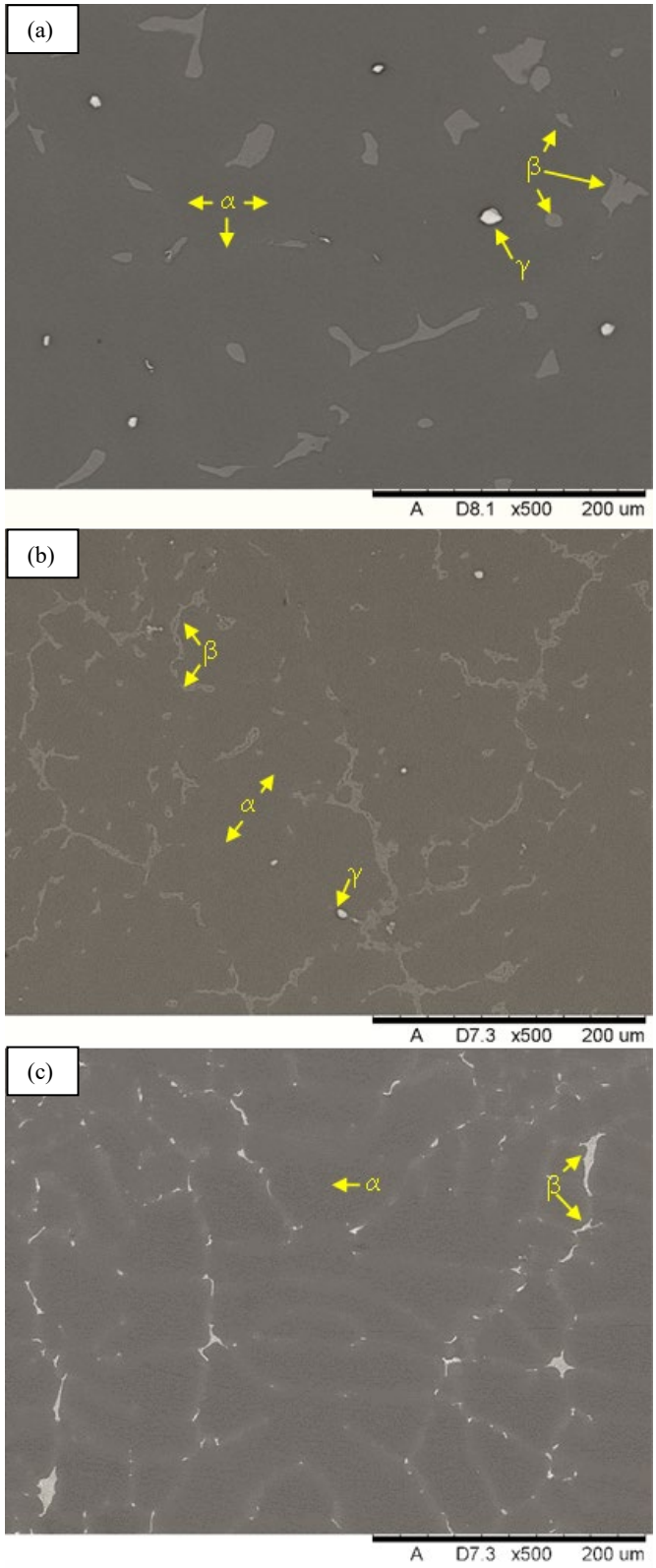


Fig. 1. Microstructure after the casting process of the surface of the samples – (a) AZ91 (AC), (b) AZ91 (SQ), (c) MgZn3

Additionally, in order to confirm the change in mechanical properties the hardness investigation has been conducted. Results presented in Table 4 show an increase in values for the AZ91 alloy after squeeze casting compared to samples after gravity casting. The same observation has been noticed in [2] where the authors analyzed Vickers microhardness. The lowest value range has been determined for the MgZn3 alloy which can be explained by the lack of Al in the chemical composition.

Table 4.
Determined Brinell hardness of investigated materials.

| AZ91 (AC) | AZ91 (SQ) | MgZn3 |
|---|---|---|
| 55 ± 2 HB | 66 ± 3 HB | 36.6 ± 1.0 HB |

The results presented in Table 3 indicate insignificant increase in $Mg_{17}Al_{12}$ phase content after squeeze casting. The similar results has been obtained in work [2], where the authors compared properties of AZ91 alloy after gravity casting, squeeze casting and extrusion. Nevertheless, in case of cited article the volume fraction has been analyzed.

Whereas, for the MgZn3 alloy, the estimated value of grain size is about 40±4 μm what is less compared to the value obtained for AZ91 after gravity casting. It must be added here that the addition of zinc to pure magnesium until 5 wt.% can efficiently refine the grain size of Mg matrix. Figure 1c provides white island-like areas distributed along grain boundary which correspond to the intermetallic β-MgZn phase. The chemical composition of its has been determined by EDS analysis, which showed the following result – 47.5 wt.% Mg and 52.5 wt.% Zn which corresponds to the characteristic atomic ratio (7:3) of the $Mg_7Zn_3$ phase. Considering the binary alloy phase diagram [27], $Mg_7Zn_3$ may conduct eutectic reaction at temperature 325 °C and decompose into α-Mg and intermetallic MgZn during cooling stage [4].

## 3.2 Electrochemical measurements

Figure 2 and Table 5 provide LSV measurements and Tafel analysis results, which show greater corrosion potential and lower corrosion rate for AZ91 (SQ) after squeeze casting compared to the same alloy manufactured by gravity casting (AZ91 (AC)). It implies that AZ91 (SQ) has better corrosion resistance in the analyzed environment (3.5 % NaCl aqueous solution). It should be noted that the obtained corrosion rate and corrosion current density values are one order lower.

It shows the influence of microstructure and refinement on corrosion resistance. As compared and mentioned above after the squeeze casting process, the microstructure is more refined and β-$Mg_{17}Al_{12}$ phase has the form of a continuous network which reduces galvanic couple effect.

Similar results have been obtained in the work cited above [2] by Marodkar et al. who drew the same conclusion based on their immersion test and potentiodynamic polarization test. Their corrosion potential values are comparable to these presented in Table 5. But their corrosion rate values determined for 72 h immersion are lower – it means 3.0 mm/year and 0.49 mm/year for AZ91 after gravity and squeeze casting, respectively. It can be explained though forming a protective film

of $Mg(OH)_2$ during immersion and it must be added here that LSV measurements and Tafel analysis are accelerated investigation in contrast to immersion test. Nevertheless, the findings in that work and the results displayed in Table 5 indicate the same conclusion as above.

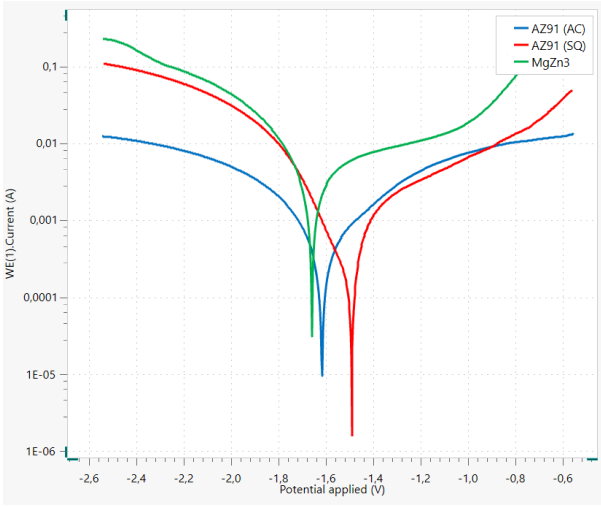


Fig. 2. Potentiodynamic polarization curve of tested materials

Furthermore, results summarized in Table 5 obtained based on Figure 2 indicate that analyzed AZ91 alloys have higher corrosion resistance in comparison to MgZn3 what can be explained by lack of $Mg_{17}Al_{12}$ phase. It should be emphasized that corrosion rate values for AZ91 (AC) and MgZn3 are very close to each other.

Table 5.
Tafel analysis results describing corrosion behavior of tested materials in 3.5 % NaCl solution.

| Material | $E_{corr}$ [V] | $j_{corr}[\frac{\mu A}{cm^2}]$ | $V_c[\frac{mm}{year}]$ |
|---|---|---|---|
| AZ91 (AC) | - 1.614 | 242.6 | 10.7 |
| AZ91 (SQ) | - 1.488 | 76.4 | 3.3 |
| MgZn3 | - 1.657 | 281.6 | 12.5 |

EIS spectra have been presented though Nyquist plot (Figure 3) and proposed equivalent electrical circuit model for them has been shown in Figure 4. Estimated values of its parameters have been provided in Table 6.

The shape of obtained curves in Figure 3 implies particular elements in the circuit model. It can be noticed a high frequency capacity loop which implies a constant phase element and a resistance of double layer (Rct). Furthermore, it can be seen a low frequency inductance loop. Due to a change in the sign of a imaginary part of impedance a inductance element L must be present in the electrical circuit model. Rs represents electrolyte resistance. It should be underlined that for all tested materials, the same circuit model could be proposed.

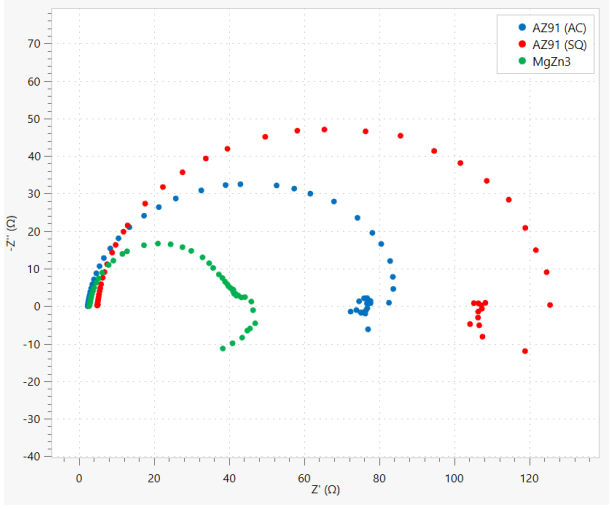


Fig. 3. Nyquist plot of investigated materials in 3.5% NaCl solution

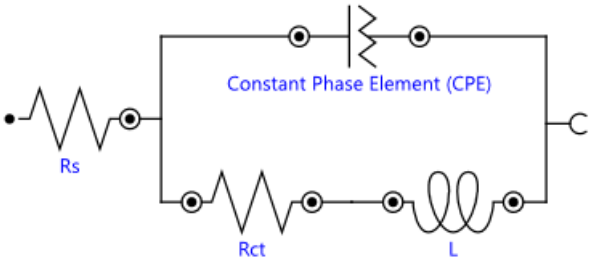


Fig. 4. Proposed equivalent electrical circuit for obtained Nyquist plot. Type [R(Q[RL])]

For employed model with an increase in the value of Rct the corrosion resistance increases. Based on obtained values in Table 6 it must be stated that AZ91 (SQ) provides the best corrosion behavior in this comparation what confirms above conclusion based on LSV measurements. Furthermore, the value of L element can also positively influence on corrosion resistance though increasing imaginary part of impedance according to the following equation:

$$X_L = j\omega L\ [\Omega] \quad (1)$$

Considering the value of N parameter describing CPE, it should be added that when N = 1 CPE behaviors as a capacitor and when N = 0.5 CPE behaviors as a Warburg impedance which concerns diffusion-controlled processes. During magnesium corrosion gas hydrogen forms and desorbs from alloy surface. Additionally, the parameter N is instrumental in evaluating surface roughness — with N = 1 indicating a smooth, polished surface, whereas values approaching zero suggest increased roughness.

During the fitting of an equivalent circuit the different models have been tested. Nevertheless, the most exact values of the parameters have been obtained for the model presented in Figure 4. For instance, the configuration type [Rs(Q[Rct(LR)])]

proposed in [1] for AZ91 alloy has been employed where an additional resistor is connected in parallel with the inductor L. Apart from that, the more complicated model has been taken into consideration. In [11] for similar curve shapes in the obtained Nyquist plot the authors prepared circuit consisting of seven elements – type [R([R(QR)](Q[RL]))]. However, in these cases obtained errors for estimated values of electrical parameters were too high to accept these models.

Additionally, Figure 5 displays the Bode plots for each material with fitting lines ascertained by the determined values which have been presented in Table 6 above.

Table 6.
Estimated values of equivalent electrical circuit parameters for presented model in 3.5 % NaCl solution.

| Parameters | Unit | AZ91 (AC) | AZ91 (SQ) | MgZn3 |
|---|---|---|---|---|
| Rs | [Ω] | 2.37 | 4.88 | 2.78 |
| Rct | [Ω] | 76.3 | 108 | 40.2 |
| L | [mH] | 26.4 | 45.8 | 46.9 |
| Y0* | [μMho*s$^N$] | 205 | 213 | 343 |
| N* | [-] | 0.899 | 0.907 | 0.868 |

* Parameters describing CPE

$$Mg + 2\,H_2O \rightarrow Mg(OH)_2 + H_2 \uparrow \quad (2)$$

$$Mg(OH)_2 + 2\,Cl^- \rightarrow MgCl_2 + 2\,OH^- \quad (3)$$

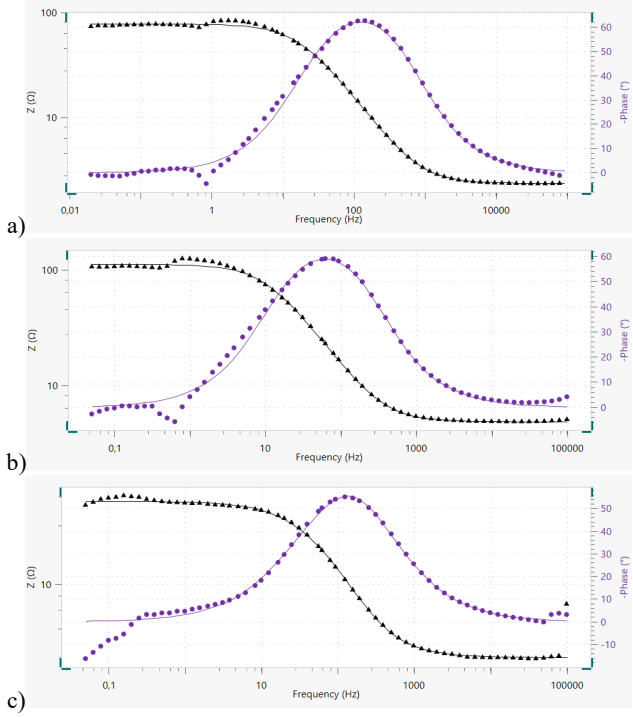


Fig. 5. Bode plots with fitting line ascertained by values provided in Table 6 for (a) AZ91 (AC), (b) AZ91 (SQ), (c) MgZn3

It must be added that in investigated corrosion environment for magnesium alloys the reactions below take place. Magnesium hydroxide is predominantly generated as a result of corrosion processes and can act as a protective layer that somewhat reduces further corrosion. However, chloride ions react with $Mg(OH)_2$ forming magnesium chloride which is more readily soluble in water and also hydroxyl ions which alkalize the aqueous solution [21, 35].

# 4. Conclusions

Based on conducted investigations the following conclusions can be formulated:

- Electrochemical measurements indicate that corrosion resistance of tested materials in 3.5 % NaCl solution at room temperature follows the order AZ91(SQ) > AZ91 (AC) > MgZn3. • The AZ91 alloy manufactured by squeeze casting demonstrates the highest corrosion potential and the least corrosion rate which is one order lower compared to other alloys. It should be emphasized that corrosion potential and corrosion rate values for AZ91 (AC) and MgZn3 are very close to each other. The factors influencing this situation should be sought in the microstructure and chemical composition of the tested alloys.
- Obtained SEM images indicate that squeeze casting refines the microstructure of the AZ91 alloys that contains the $Mg_{17}Al_{12}$ phase. For samples obtained by this process this phase is in a form of continuous network distributing along the gain boundary. For samples manufactured by gravity casting it is bulky and separated which reduces corrosion resistance (increases corrosion rate value) due to galvanic couple effect.
- The addition of Zn to pure magnesium can efficiently refine the grain size of Mg matrix. Formed MgZn phase creates an extensive network distributing along the gain boundary. It can be stated that the microstructure is similar to that in the case of AZ91 after squeeze casting and it can be expected low corrosion rate. However, lack of Al has a negative impact on corrosion resistance in the analyzed environment compared to AZ series alloys.
- Obtained corrosion rate values for all investigated materials are greater than 1.0 mm/year. Therefore they should be classified as materials that are not resistant to corrosion in tested conditions.
- For analyzed corrosion system the most suitable electrical equivalent circuit has been proposed and values of its parameters have been estimated.

# Acknowledgements

This work has been developed in the frame of the CERMET project, funded by the National Centre for Research and Development POLTAJ10/2022/53/CERMET/2023 (Poland) and National Science and Technology Council 112-2923-E-027 -001 - MY3 (Taiwan).

# References


[1] Madhavan, A.S., Thomas, K.A., & Rajith, L. (2025). Electrochemical characterization and discharge performance of AZ31, AZ61 and AZ91 alloys as anodes for seawater battery. *Journal of Power Sources.* 628, 235863, 1-13. https://doi.org/10.1016/j.jpowsour.2024.235863.

[2] Marodkar, A.S., Patil, H., Chavhan, J. & Borkar, H. (2023). Effect of gravity die casting, squeeze casting and extrusion on microstructure, mechanical properties and corrosion behaviour of AZ91 magnesium alloy. *Materials Today*: *Proceedings*. 1-9. https://doi.org/10.1016/j.matpr.2023.03.053.

[3] Zhang, S., Zhang, X., Zhao, C., Li, J., Song, Y., Xie, C., Tao, H., Zhang, Y., He, Y., Jiang, Y. & Bian, Y. (2010). Research on an Mg-Zn alloy as a degradable biomaterial. *Acta Biomaterialia.* 6(2), 626-640. https://doi.org/10.1016/j.actbio.2009.06.028.

[4] Cai, S., Lei, T., Li, N. & Feng, F. (2012). Effects of Zn on microstructure, mechanical properties and corrosion behavior of Mg-Zn alloys. *Materials Science and Engineering C*. 32(8), 2570-2577. https://doi.org/10.1016/j.msec.2012.07.042.

[5] Bankoti, A.K.S., Mondal, A.K., Perugu, C.S., Ray, B.C. & Kumar, S. (2017). Correlation of microstructure and electrochemical corrosion behavior of squeeze-cast Ca and Sb added AZ91 Mg alloys *Metallurgical and Materials Transactions A.* 48(10), 5106-5121, https://doi.org/10.1007/s11661-017-4244-1.

[6] Yang, J., Peng, J., Nyberg, E.A. & Pan, F.S. (2016). Effect of Ca addition on the corrosion behavior of Mg–Al–Mn alloy. *Applied Surface Science.* 369, 92-100, https://doi.org/10.1016/j.apsusc.2016.01.283.

[7] Powell, B.R., Krajewski, P.E. & Luo, A.A. (2010). Magnesium alloys for lightweight powertrains and automotive structures. *Materials, Design and Manufacturing for Lightweight Vehicles.* 80, 114-173. https://doi.org/10.1533/9781845697822.1.114.

[8] Staiger, M.P. Pietaka, A.M., Huadmaia, J. & Dias, G. (2006) Magnesium and its alloys as orthopedic biomaterials: A review. *Biomaterials.* 27(9), 1728-1734. https://doi.org/10.1016/j.biomaterials.2005.10.003.

[9] Song, G. & Atrens, A. (2003). Understanding magnesium corrosion—a framework for improved alloy performance. *Advanced Engineering Materials.* 5(12), 837-858. https:// doi.org/10.1002/adem.200310405.

[10] Saidov, S., Tselovalnik, Y. V., Belov, V. D. & Bazhenov, V. E. (2021). Comparison of castability, mechanical, and corrosion properties of Mg-Zn-Y-Zr alloys containing LPSO and W phases. *Transactions of Nonferrous Metals Society of China.* 31, 1276–1290. https://doi.org/10.1016/S1003-6326(21)65577-2.

[11] Li, Z., Peng, Z., Qi, K., Li, H., Qiu, Y. & Guo, X. (2020). Microstructure and corrosion of cast magnesium alloy ZK60 in NaCl solution. *Materials.* 13(17), 3833, 1-21. https://doi.org/10.3390/ma13173833.

[12] Song, G.L., Atrens, A. & Dargusch, M. (1998). Influence of microstructure on the corrosion of diecast AZ91D. *Corrosion Science.* 41(2), 249-273. https://doi.org/10.1016/S0010-938X(98)00121-8.

[13] Song, G.L., Atrens, A., St John, D., Li, Z. (2000). *Magnesium alloys and their applications*. Germany: Wiley–VCH: Weinheinm.

[14] Mordike, B.L. & Ebert, T. (2001). Magnesium properties — applications — potential. *Materials Science and Engineering A.* 302(1), 37-45. https://doi.org/10.1016/S0921-5093(00)01351-4.

[15] Marodkar, A.S., Patil, H., Borkar, H. & Behl, A. (2023). Effect of squeeze casting and combined addition of calcium and strontium on microstructure and mechanical properties of AZ91 magnesium alloy. *International Journal of Metalcasting.* 17, 2252-2270. https://doi.org/10.1007/s40962-022-00943-1.

[16] Urtekin, L., Ozerkan, H.B., Cogun, C., Genc, A., Esen, Z. & Bozkurt, F. (2021). Experimental investigation on wire electric discharge machining of biodegradable AZ91 Mg alloy. *Journal of Materials Engineering and Performance.* 30(10), 7752-7761. https://doi.org/ 10.1007/s11665-021-05939-2.

[17] Czerwinski, F. (2014). Controlling the ignition and flammability of magnesium for aerospace applications. *Corrosion Science.* 86, 1-16, https://doi.org/10.1016/ j.corsci.2014.04.047.

[18] Huang, S.J., Diwan Midyeen, S., Subramani, M. & Chiang, C.C. (2021). Microstructure evaluation, quantitative phase analysis, strengthening mechanism and influence of hybrid reinforcements (b-SiCp, Bi and Sb) on the collective mechanical properties of the AZ91 magnesium matrix. *Metals.* 11(6), 898, 1-21. https://doi.org/10.3390/met11060898.

[19] Tolouie, E. & Jamaati, R. (2018). Effect of β–$Mg_{17}Al_{12}$ phase on microstructure, texture and mechanical properties of AZ91 alloy processed by asymmetric hot rolling. *Material Science Engineering A.* 738, 81-89. https://doi.org/10.1016/j. msea.2018.09.086.

[20] Lv, X., Deng, K.K., Wang, C.J., Nie, K.B., Shi, Q.X. & Liang, W. (2022). The corrosion properties of AZ91 alloy improved by the addition of trace submicron SiCp. *Materials Chemistry and Physics.* 286, 126143, 1-14. https://doi.org/10.1016/j.matchemphys.2022.126143.

[21] Song, G.L. & Atrens, A. (1999). Corrosion mechanisms of magnesium alloys. *Advanced Engineering Materials.* 1(1), 11-33. https://doi.org/10.1002/(SICI)1527-2648(199909)1:1%3C11::AID-ADEM11%3E3.0.CO;2-N.

[22] Koc, E. (2019). Corrosion behaviour of as cast β-$Mg_{17}Al_{12}$ phase in 3.5 wt% NaCl solution. *Acta Physica Polonica.* 135(5), 881-883. https://doi.org/10.12693/ APhysPolA.135.881.

[23] Ambat, R., Aung, N.N. & Zhou, W. (2000). Evaluation of microstructural effects on corrosion behaviour of AZ91D magnesium alloy. *Corrosion Science.* 42(8), 1433-1455. https://doi.org/10.1016/S0010-938X(99)00143-2.

[24] Zhang, T., Li, Y. & Wang, F. (2006). Roles of b phase in the corrosion process of AZ91D magnesium alloy. *Corrosion Science.* 48(5), 1249-1264. https://doi.org/ 10.1016/j.corsci.2005.05.011.

[25] Song, G. (2013). Corrosion behavior and prevention strategies for magnesium (Mg) alloys. *Corrosion prevention of magnesium alloys.* 3-37. https://doi.org/10.1533/9780857098962.1.3.
[26] Song, Y.L., Liu, Y.H., Wang, S.H., Yu, S.R. & Zhu, X.Y. (2007). Effect of cerium addition on microstructure and corrosion resistance of die cast AZ91 magnesium alloy, *Materials and Corrosion.* 58(3), 189-192. https://doi.org/10.1002/maco.200603988.
[27] Okamoto, H. (1994). Comment on Mg–Zn (magnesium–zinc). *Journal of Phase Equilibria.* 15(1), 129-130. https://doi.org/10.1007/BF02667700.
[28] Boehlert, C.J. & Knittel, K. (2006). The microstructure, tensile properties, and creep behavior of Mg-Zn alloys containing 0-4.4 wt.% Zn. *Materials Science and Engineering: A*. 417(1-2), 315-321. https://doi.org/10.1016/j.msea.2005.11.006.
[29] Dmitruk, A., Naplocha, K., Żak, A. & Strojny-Nędza, A. (2024). Refinement of the manufacturing route and evaluation of the reinforcement effect of MAX phases in Al alloy matrix composite materials. *Archives of Foundry Engineering.* 24(1), 141-148. https://doi.org/10.24425/afe.2024.149262.
[30] Kapłon, H., Dmitruk, A. & Naplocha, K. (2023). Investment casting of AZ91 magnesium open-cell foams. *Archives of Foundry Engineering.* 23(1), 11-16. https://doi.org/10.24425/afe.2023.144274.
[31] Cubides, Y., Ivan Karayan, A., Vaughan, M.W., Karaman, I. & Castaneda, H. (2020). Enhanced mechanical properties and corrosion resistance of a fine-grained Mg-9Al-1Zn alloy: the role of bimodal grain structure and β-Mg17Al12 precipitates. *Materialia.* 13, 100840, 1-19. https://doi.org/10.1016/j.mtla.2020.100840.
[32] Zhang, Y., Wu, G., Liu, W., Zhang, L., Pang, S., Wang, Y. & Ding, W. (2014). Effects of processing parameters and Ca content on microstructure and mechanical properties of squeeze casting AZ91–Ca alloys. *Materials Science and Engineering A*. 595, 109-117. https://doi.org/10.1016/j.msea.2013.12.014.
[33] Bai, J., Sun, Y., Xue, F. & Qiang, J. (2012). Microstructures and creep properties of Mg–4Al–(1–4) La alloys produced by different casting techniques. *Materials Science and Engineering A.* 552, 472-480. https://doi.org/10.1016/j.msea.2012.05.072.
[34] Yu, H., Chen, S.N., Yang, W., Zhang, Y.L. & Chen, S.H. (2014). Effects of rare element and pressure on the microstructure and mechanical property of AZ91D alloy. *Journal of Alloys and Compounds.* 589, 479-484. https://doi.org/10.1016/j.jallcom.2013.12.019.
[35] Xin, Y., Liu, C., Zhang, X., Tang, G., Tian, X. & Chu, P. (2007). Corrosion behavior of biomedical AZ91 magnesium alloy in simulated body fluids. *Journal of Materials Research.* 22, 2004-2011. https://doi.org/10.1557/jmr.2007.0233.